nature geoscience

Article

https://doi.org/10.1038/s41561-024-01422-4

Weakening of the Atlantic Meridional Overturning Circulation abyssal limb in the North Atlantic

Received: 26 June 2023

Accepted: 15 March 2024

Published online: 19 April 2024

Check for updates

Tiago Carrilho Biló[1,2] ✉, Renellys C. Perez[2], Shenfu Dong[2], William Johns[3] & Torsten Kanzow[4,5]

The abyssal limb of the global Meridional Overturning Circulation redistributes heat and carbon as it carries Antarctic Bottom Water from the Southern Ocean towards the Northern Hemisphere. Using mooring observations and hydrographic data from multiple sources in the North Atlantic, we show that northward-flowing Antarctic Bottom Water is constrained below 4,500 m with a mean volume transport of 2.40 ± 0.25 Sv at 16° N. We find that during 2000–2020, the Antarctic Bottom Water northward transport weakened by approximately 0.35 ± 0.13 Sv, corresponding to a 12 ± 5% decrease. The weakening of the Atlantic Meridional Overturning Circulation abyssal cell is a probable response to reduced Antarctic Bottom Water formation rates over the past several decades and is associated with abyssal warming observed throughout the western Atlantic Ocean. We estimate that the warming of the Antarctic Bottom Water layer in the subtropical North Atlantic is, on average, 1 m°C per year in the last two decades due to the downward heaving of abyssal isopycnals, contributing to the increase of abyssal heat content and, hence, sea-level rise in the region (1 m°C = 0.001 °C). This warming trend is approximately half of the Antarctic Bottom Water warming trend observed in the South Atlantic and parts of the Southern Ocean, indicating a dilution of the signal as the Antarctic Bottom Water crosses the Equator.

The Antarctic Bottom Water (AABW) forms through a myriad of physical processes along the Antarctic continent, comprising the world's oceans' coldest and densest water masses[1]. As it spreads northward, it redistributes large amounts of heat and carbon within the deepest limb of the global Meridional Overturning Circulation (MOC)[2], filling most of the ocean's deep (1,000 < depth < 4,000 m) and abyssal (depth > 4,000 m) areas[3]. Therefore, water temperature and circulation variations within this cold but vast water reservoir have a global impact on Earth's heat budget[4,5] and sea-level rise[6,7].

The AABW has significantly warmed since the 1980s around the globe, with the observed warming rates up to 5 m°C per year near the AABW's formation sites[6,8–15] (1 m°C = 0.001 °C). In certain regions such as the Australian Antarctic Basin, there is evidence of AABW warming and freshening starting much earlier in the 1960s[16]. Analysis of repeated hydrography surveys suggests that this warming is associated with the downward displacement of isopycnals, indicating a potential decrease of the AABW's total volume in the abyssal oceans consistent with the reduction in AABW's formation rates in the past five decades[17].

[1]Cooperative Institute for Marine and Atmospheric Studies, Rosenstiel School of Marine, Atmospheric and Earth Science, University of Miami, Miami, FL, US. [2]Atlantic Oceanographic and Meteorological Laboratory, National Oceanic and Atmospheric Administration, Oceanic and Atmospheric Research, Miami, FL, US. [3]Rosenstiel School of Marine, Atmospheric and Earth Science, University of Miami, Miami, FL, US. [4]Climate Sciences Division, Alfred-Wegener-Institute Helmholtz Center for Polar and Marine Research, Bremerhaven, Germany. [5]Department of Physics and Electrical Engineering, University of Bremen, Bremen, Germany. ✉e-mail: tiago.bilo@noaa.gov

https://doi.org/10.1038/s41561-024-01422-4

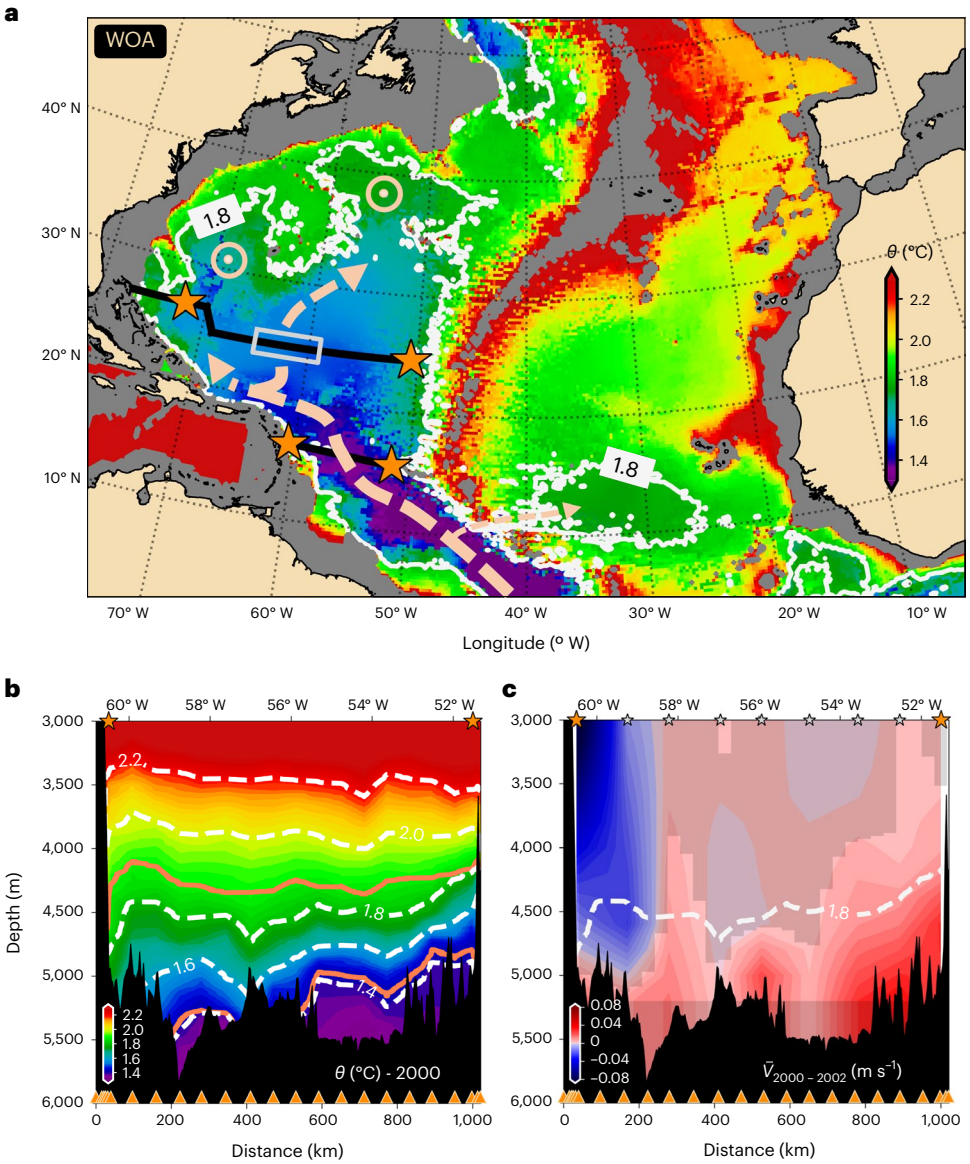

Fig. 1 | AABW distribution and its primary pathways in the North Atlantic. **a**, World Ocean Atlas (WOA) potential temperature θ values closest to the bottom of the North Atlantic tropical and subtropical regions overlayed with the AABW flow (that is, $\theta < 1.8$ °C) direction and deep upwelling areas based on ref. 29 (dashed arrows and circles, respectively). The stars indicate the mooring locations from the Meridional Overturning Variability Experiment (MOVE, 16° N), Rapid Climate Change Meridional Overturning Circulation (RAPID, 24.5° N) and Western Boundary Current Time Series (WBTS, 26.5° N) programmes. The black line along 16° N represents the CTD transects from the MOVE programme and where the Guyana Abyssal Gyre Experiment (GAGE) moorings were also located. The black line farther north is the approximate location of the World Ocean Circulation Experiment-International Global Ocean Ship-Based Hydrography Investigations Program (WOCE-GOSHIP) CTD transects (that is, A05 line). The grey box bounds the mid-basin area where Deep Argo profiles are present along 24.5° N (65° W–59° W). Areas shallower than 3,000 m have been masked in grey. **b**, Abyssal θ transect (colour scales and dashed lines) obtained during the MOVE moorings (orange stars) deployment cruise in 2000 at 16° N, overlayed with neutral density (γ_n) = 28.110 and 28.135 kg m^{-3} isopycnals (solid orange lines). **c**, Cross-transect 2000–2002 mean velocity from the GAGE programme overlayed with $\theta = 1.8$ °C isotherm from the MOVE 2000 cruise (dashed white line). The dark shade indicates the areas where the uncertainty of the mean velocity surpasses the signal within the 95% confidence interval (that is, 2 × standard error; sample size = 403). Positive velocities are northward. Orange stars and triangles in **b** and **c** represent the MOVE moorings and CTD casts locations at 16° N, respectively. Grey and orange stars in **c** are the GAGE moorings locations.

Both data assimilation[7,18] and non-assimilative numerical experiments[19,20] suggest that a decrease in the AABW formation rates and, consequently, a slowdown of the northward AABW flow could trigger a series of Kelvin and Rossby waves that can bring such anomalies to northern areas of the oceanic basins on decadal timescales[18,19] instead of the expected advective travel times of hundreds to thousands of years[21]. Specifically in the Atlantic Ocean, where the primary AABW source is the Weddell Sea[22,23], ref. 20 showed that this simulated fast oceanic response to changes around the Southern Ocean is not only associated with the possible weakening and warming of the northward abyssal limb of the Atlantic MOC (AMOC) but also with the acceleration of the flow within the deep and upper layers of the AMOC. Although the northward progression of the warming signal could be partially explained by the advection of the slow abyssal flow, ref. 20 verified that the onset of the quasi-linear warming trends in the Vema Channel at 30° S (also present in observations since the late 1970s[24]) and northward is probably explained by the wave response. Whereas this dynamic ocean adjustment process is a robust feature of different types of numerical simulation, suggesting the ongoing climate change will continue to induce the global abyssal ocean to warm for

https://doi.org/10.1038/s41561-024-01422-4

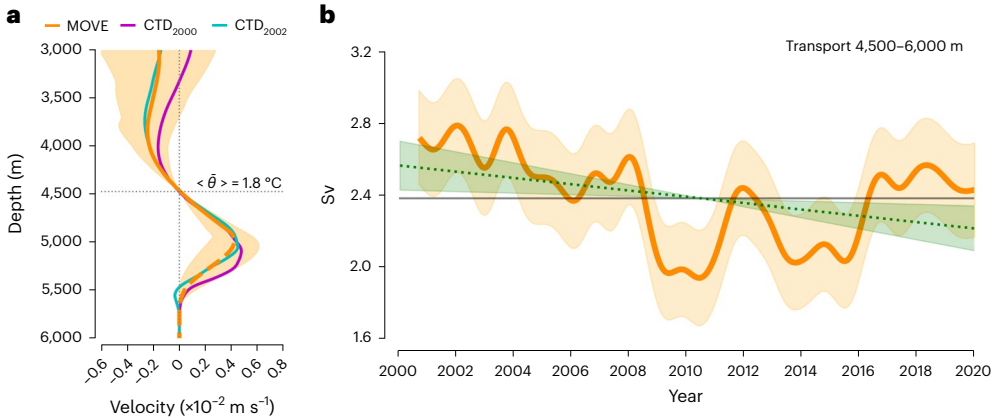

Fig. 2 | MOVE data analysis showing the AABW flow weakening in the twenty-first century at 16° N. a, Mooring-based 2000–2020 mean (orange line) and CTD-based (magenta and cyan lines) geostrophic velocity profiles between the MOVE moorings referenced at 4,500 m. Positive velocities are northward. The dashed portion of the mooring-based profile shows where our vertical extrapolation scheme was applied. The shaded area is the mooring-based geostrophic velocity data range throughout the time series at each depth (sample size = 7,341 data points). Finally, the horizontal dotted line is the average depth of the 1.8 °C isotherm ($< \bar{\theta} >$) calculated from the CTD transects. **b**, Eighteen-month low-passed filtered AABW geostrophic transports referenced at and integrated between 4,500 and 6,000 m. The solid and dotted lines are the mean transport and the transport linear trend, respectively. Shaded areas around the curves represent the transport and its linear trend uncertainties within 95% confidence intervals of our calculations (that is, 2 × standard error). Whereas the linear trend uncertainty was calculated using all 7,341 data points, the standard errors of the transport correspond to the standard errors within a one-year-long running window (that is, 365 data points).

the foreseeable future[25], observational studies of the abyssal North Atlantic have reported vigorous variability showing no evidence of statistically robust long-term trends after 2000[26,27].

The AABW enters the North Atlantic Basin primarily between the South American continent and the Mid-Atlantic Ridge (MAR) below the North Atlantic Deep Water (NADW) and reaches as far poleward as 40° N (see 1.8 °C isotherm, or AABW and NADW interface, in Fig. 1a). Although part of this abyssal flow could penetrate the basin's eastern side through large fracture zones along the MAR, the bulk of AABW continues to spread to the west of the MAR[9,28–30]. North of 16° N, measurements from multiple repeated hydrographic transects in the western North Atlantic obtained between 1981 and 2004 indicated that the AABW volume reduced by up to 30–40% during this period[9], suggesting a possible halt of the AABW inflow to the North Atlantic Ocean in the coming decades. Although abyssal geostrophic transport estimates at 24.5° N from repeated hydrographic surveys corroborated the results of ref. 9, the same dataset extended between 1957 and 2010 plus six months of moored records showed that the AABW geostrophic transports exhibit variability from daily to interannual timescales[26], making it difficult to ascertain any longer-term AABW transport trends, especially after 1998. Additionally, these repeated surveys up to 2004 revealed that cooling along isopycnal surfaces associated with abyssal freshening surpassed the abyssal warming signal driven by the contraction of the AABW cold layer[31]. Finally, recent temperature analyses of the entire abyssal western North Atlantic between 4,000 and 6,000 m indicated that these areas slightly cooled between 2000 and 2014 due to both abyssal freshening and vertical expansion of the abyssal layers[27], opposing the observed North Atlantic's 1980s–2000 and South Atlantic's 1970s–present warming tendencies[6,9,10,15,24,26,32]. Although some of the cited hydrographic changes associated with small salinity variations observed before 2000 should be interpreted with caution due to larger uncertainties[33], the vigorous abyssal temperature and transport variability at different timescales reported by multiple studies put into question the persistence of the slowdown of the abyssal AMOC and its associated warming in the North Atlantic basin in the twenty-first century.

In the present study, we use moored hydrographic observations, multiple hydrographic cruise surveys and Deep Argo profiles (Fig. 1a) to quantify the variability of the AABW inflow to the subtropical North Atlantic on interannual to longer timescales and the associated abyssal warming trends in the first two decades of the twenty-first century. We found robust observational evidence for a persistent kinematic weakening of the AMOC's abyssal limb in the North Atlantic Ocean between 2000 and 2020, suggesting that the AABW formation and volume reduction signal in the Southern Hemisphere continuously penetrated the region during that period, increasing the abyssal heat content and contributing to the sea-level rise.

Weakening of the North Atlantic abyssal circulation

Across 16° N, the northward-flowing AABW layer is mainly limited to below 4,500 m (Fig. 1b). Most of the AABW seems to be flowing northward within the abyssal current above the western flank of the MAR with maximum velocities of about 3–4 × 10^{-2} m s^{-1} below 5,000 m (Fig. 1c), in agreement with observations[26,31,34–36] and idealized simulations[37] of the abyssal flow in the Atlantic Ocean. Not surprisingly, geostrophic velocity profiles relative to 4,500 m averaged across this area reveal that the northward flow increases with depth below 4,500 m, peaks between 5,000 and 5,200 m and then decreases to approximately zero between ~5,500 and 5,800 m (Fig. 2a). Integrating the abyssal geostrophic velocity along 16° N and below 4,500 m, we find a mean AABW transport of 2.40 ± 0.25 Sv. The hydrographic mooring observations also indicate that the AABW transport is weakening at a rate of 1.75 ± 0.65 × 10^{-2} Sv per year since 2000 (Fig. 2b). Over approximately 20 years, the AABW transport reduced by 0.35 ± 0.13 Sv, corresponding to 12 ± 5% of the annual mean transport in 2000. Besides the significant long-term trend, the abyssal transports exhibit substantial interannual variability. The most prominent events are the strong decrease in 2008–2010 of 0.65 Sv and the 0.50 Sv transport recovery in 2016–2017.

Because we referenced our mooring-based geostrophic transport estimates to a constant depth (Methods), their variability mainly arises from changes in the vertical geostrophic shear, which are proportional to horizontal density gradient variations across 16° N. The observed 20-year-long AABW transport reduction (Fig. 2b) resulted from the decrease of the geostrophic shear below ~4,600 m (Fig. 3a). Because the isotherms and isopycnals within the AABW layer tend to rise eastward (Fig. 1b,c), a warming/freshening of AABW near the western flank of the MAR would act to flatten the isopycnals and, consequently, weaken the abyssal geostrophic flow. We find that the abyssal warming near the MAR is the primary contributor to the isopycnal flattening associated

https://doi.org/10.1038/s41561-024-01422-4

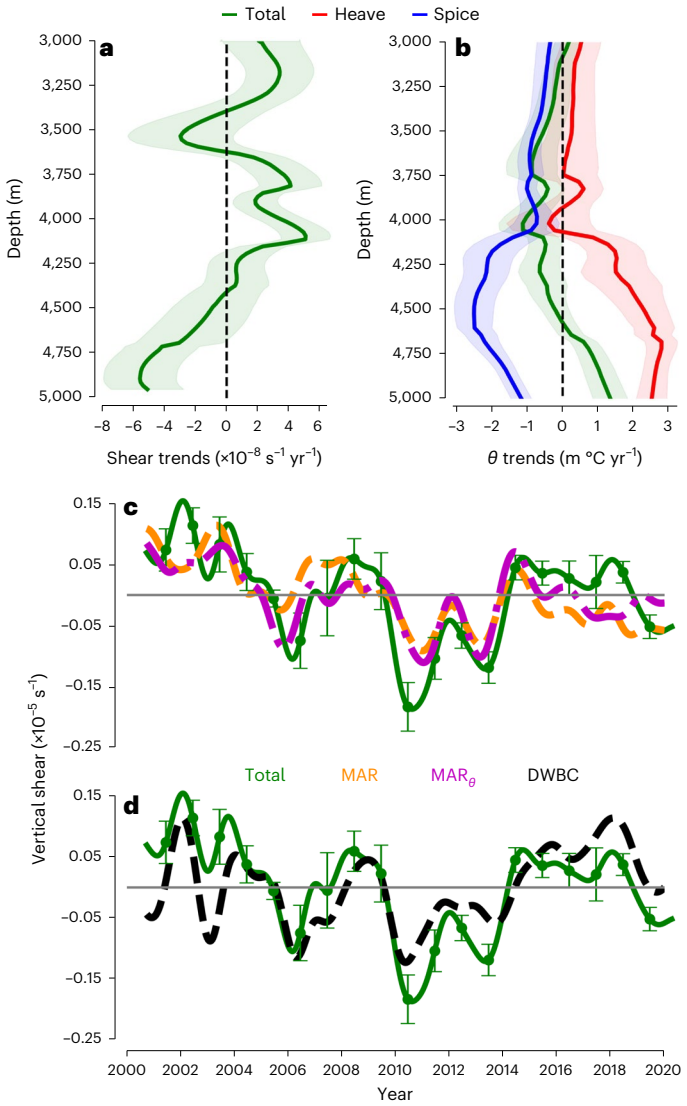

Fig. 3 | MOVE data analysis showing that warming due to isopycnal heaving near the MAR decreased the abyssal geostrophic shear at 16° N. a, The 2000–2020 linear geostrophic shear trends. **b**, The 2000–2020 linear θ trends (green line) near the MAR and their decomposition into heave (red line) and spice (blue line) components. **c**,**d**, Eighteen-month low-passed filtered abyssal geostrophic shear time anomalies averaged between 4,500 and 5,000 m (solid green line) and its correspondent variability sources: density changes near the MAR (orange dashed line), temperature changes near the MAR (MAR_θ, magenta dashed line) and density changes within the DWBC domain (DWBC, dashed black line). The sum of MAR and DWBC curves corresponds to the total shear. Uncertainties, shown as shaded areas and error bars, represent the 95% confidence intervals (2 × standard error) around each curve. Whereas the linear trends' uncertainties in **a** and **b** were calculated using all 7,341 data points, the vertical shear standard errors in **c** and **d** correspond to the standard errors within an one-year-long running window (that is, 365 data points).

with the long-term weakening of the AABW transport. Whereas the vertical shear (Fig. 3c, solid green line) is decreasing at a rate approximately the same as the shear due to the warming near the MAR (that is, about $-3.8 \pm 1 \times 10^{-8}$ s^{-1} per year) (Fig. 3c, dashed magenta line), the density changes within the Deep Western Boundary Current (DWBC) (that is, NADW flow) impose a prominent multi-decadal oscillation to the shear, but no significant trend was detected between 2000 and 2020 (Fig. 3d, dashed black line). In contrast, the interannual to decadal abyssal shear variability, and consequently the AABW transport variability, is mainly explained by the density variations at the DWBC with smaller but notable contributions from the western flank of MAR (Fig. 3c,d). The variability at the DWBC explains approximately 80% of the detrended shear variance, generating shear anomalies that are highly correlated with the observed total shear anomalies (Extended Data Fig. 1).

Like the shear and transport trends, the warming trend near the MAR is statistically significant below 4,600 m, and its magnitude increases with depth, reaching rates of about 1.50 ± 0.25 m°C per year near 5,000 m (green line in Fig. 3b). Additionally, downward isopycnal heaving is the mechanism responsible for warming, further suggesting the weakening of the AABW flow is associated with the shrinking of this bottom water layer (red line in Fig. 3b). Notably, cooling along isopycnal surfaces (also known as spice trend) indicates that the AABW has also freshened during the same period, surpassing the heaving effect above 4,500 m (blue line in Fig. 3b). The average freshening rate of the AABW layer is approximately $-2 \pm 1 \times 10^{-4}$ per year.

The North Atlantic abyssal warming

As a result of the weakening of the relatively cold and fresh AABW flow since 2000, we expect the AABW layer to shrink, warming the abyssal North Atlantic as the overlaying NADW layer vertically expands[20]. To verify this, we use the hydrographic measurements obtained between 1998 and 2022 from multiple programmes crossing the western North Atlantic basin between 24.5° N and 26.5° N (Figs. 1 and 4). Like at 16° N, the AABW layer is primarily found below 4,500 m with upward-tilted isotherms encroaching on the western flank of the MAR (Fig. 4a). In contrast, the AABW layer is notably warmer at this latitude (that is, average minimum temperatures ~0.2 °C warmer), probably due to the continuous vertical mixing with NADW as it flows northward[26,35]. Note that west of 69° W, the AABW layer thickness substantially decreases, resulting in the 1.8 °C isotherm lying close to the bottom west of 72° W consistent with the presence of the DWBC and its localized recirculation cell carrying NADW in this area[38].

As seen at 16° N, the AABW is warming below approximately 4,500 m, on average (Fig. 4b). However, the trend only becomes statistically significant near ~5,200 m (solid green line). Within the AABW layer (4,500–6,000 m), we estimate the average warming to be approximately 0.96 ± 0.56 m°C per year, which is driven by the downward heaving of the isopycnals (dashed red line). Because of the limited data covering the entire western North Atlantic basin (that is, six cruises), the trend uncertainties are larger at this latitude (shaded area). To further validate this warming trend, we analysed temperature variations over a smaller mid-basin section where several Deep Argo profiles were available and approximately evenly distributed along the conductivity, temperature and depth (CTD) line. The trends over this smaller section that combines CTD and Argo profiles (solid orange line in Fig. 4b,c) are slightly different but consistent with the signal averaged over the AABW domain, resulting in an AABW layer warming rate of ~1 m°C per year.

Note that the abyssal western North Atlantic subtropics at 24.5° N–26.5° N seems to have cooled in 2020 (Fig. 4c–e). Coincidentally, the AABW transport sharply increased between 2016 and 2017 across 16° N and remained relatively strong until 2020 (Fig. 2b) compared with previous years when observations along 24.5° N–26.5° N were available, suggesting the AABW's transport interannual variability is probably responsible for the cooling. The temperature mooring records at 16° N also indicate a concurrent cooling below 4,500 m (Extended Data Fig. 2).

The moored and CTD measurements near the lateral edges of the AABW layer do not show a statistically significant trend (Fig. 4d–e). Instead, shorter timescales dominate the temperature variability, suggesting the abyssal long-term warming is more robust closer to the core of the AABW. This spatial confinement of the warming signal could partially explain the inconsistent post-2000 temperature trends sign for broader areas of the abyssal North Atlantic estimated by previous studies[10,27] because it includes regions with larger fractions of NADW

https://doi.org/10.1038/s41561-024-01422-4

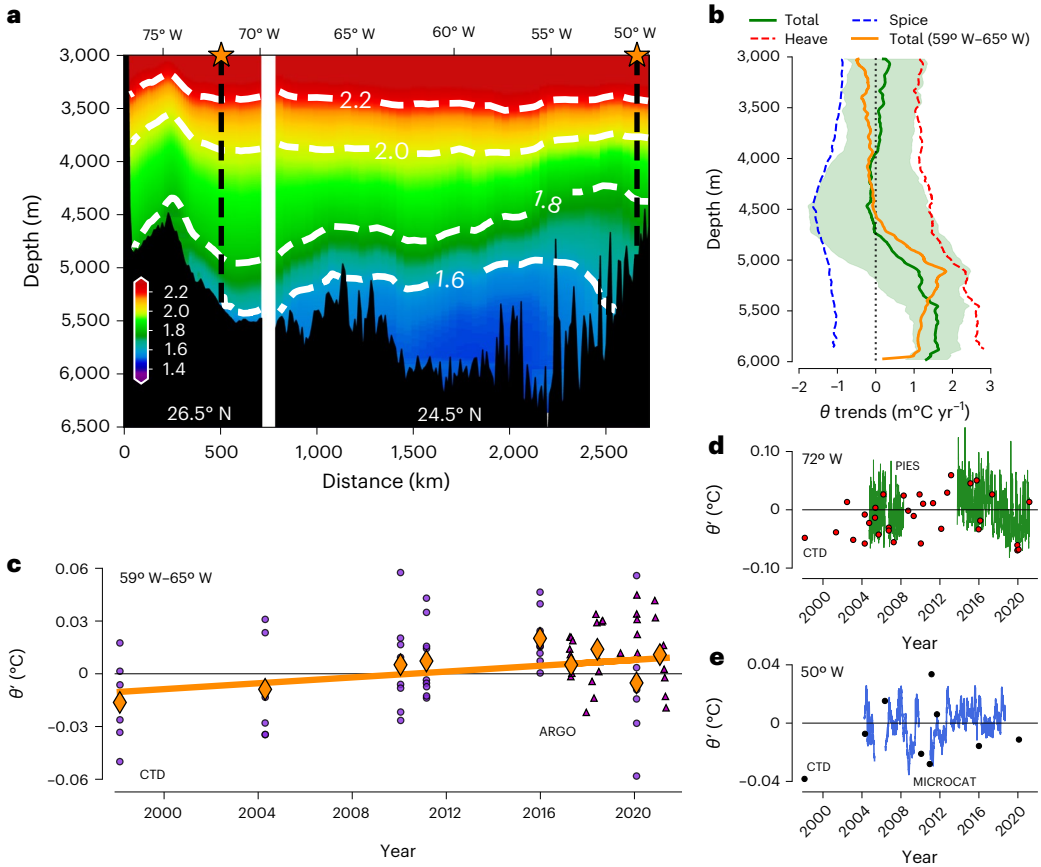

Fig. 4 | Analysis of the hydrographic observations showing the AABW distribution and its warming signal at 24.5° N–26.5° N. a, Abyssal mean θ transect calculated from CTD casts obtained as part of the WBTS, WOCE-GOSHIP and RAPID programmes between 1998 and 2020. Stars and dashed black lines indicate the WBTS' moored Pressure Equipped Inverted Echo Sounder (PIES, 72° W) and the RAPID moored MicroCATs (50° W) locations. **b**, CTD-based linear θ trends averaged across the basin along 24.5° N (solid green line) and its heave and spice components (red and blue dashed lines, respectively) overlayed with CTD + Argo-based linear θ trends between 1998 and 2022 near the centre of the basin (59° W–65° W, solid orange line). The shaded area represents the 95% confidence interval of the basin-wide total trend (that is, 2 × standard error; sample size = six data points). **c**, Vertically averaged θ anomalies below 4,500 m depth near the centre of the basin (59° W–65° W) from CTD casts (small circles) and Argo profiles (small triangles). Whereas the thick solid orange line shows the warming trend obtained by combining CTDs and Argo measurements, the large diamonds represent the zonally averaged temperature measurements. **d**,**e**, Near-bottom θ anomalies at the western and eastern edges of the AABW layer from moored records and CTD casts at the moorings' sites. Note that the *y*-axis limits are panel dependent for better visualization.

(for example, western boundary, areas east of MAR, depths between 4,000 and 4,500 m). Along the 24.5° N–26.5° N section, however, the inclusion of the hydrographic stations closer to the western boundary does not change the overall magnitude of the trend below 4,500 m but instead increases its uncertainties due to the spatial temperature variability.

Assuming the horizontally averaged constant AABW warming rate profile (green line in Fig. 4b), we estimate the western North Atlantic gained about 0.49 ZJ between 2000 and 2020, equivalent to a 0.05 W m^{-2} heat flux across 4,500 m between the Equator and 40° N (that is, northernmost AABW penetration), contributing to a sea-level rise (SLR) of 0.14 mm per year via thermal expansion (calculation details in Methods). Our western North Atlantic SLR estimates are consistent with the magnitude of the deep and abyssal warming contributions to global SLR from repeated hydrography since the 1990s[6,27], which are at least one order of magnitude smaller than the upper ocean contribution to global long-term SLR trends[27]. One should interpret these numbers as a first-order rough approximation of the abyssal warming impact on the North Atlantic because our data do not include any latitudinal variability of the temperature trends. Nevertheless, the same average warming trend applied over 20 years results in a reduction of the climatological AABW layer volume of approximately $1.7 \pm 1.0 \times 10^{14}$ m^3 north of 16° N, which agrees within uncertainties with the volume reduction suggested by the independent AABW transport estimates across 16° N (that is, $1.1 \pm 0.4 \times 10^{14}$ m^3). In addition, ref. 6 showed that the abyssal western North Atlantic ($z > 4{,}000$ m) gained heat at a similar rate between the early 1990s and early 2000s (that is, 0.05 ± 0.18 W m^{-2}) using all available hydrographic data across the basin. However, the authors estimated an uncertainty three times the warming signal. Our rough heat flux estimates further corroborate these previous long-term trend estimates and suggest the trends pre- and post-2000 are similar.

The persistent abyssal AMOC weakening

We showed that the northward-flowing AABW across 16° N is mainly constrained below 4,500 m and concentrated along the western flank of the MAR with a mean transport of 2.40 ± 0.25 Sv. This flow has weakened by approximately 0.35 Sv (that is, 12%) between 2000 and 2020, associated with an average abyssal warming of about 1 m°C per year driven by the downward heaving of the abyssal isopycnals within the AABW layer. Additionally, the AABW transport variability presents substantial interannual to decadal oscillations.

Whereas we found AABW flow patterns at 16° N that are in general agreement with previous studies across the North Atlantic[26,31,35,39], our analysis also revealed that the long-term weakening of the AABW inflow to the western North Atlantic since the 1980s[9,26] persisted up to 2020,

contributing to the increase of the abyssal heat content and, hence, sea-level rise in the region. As we mentioned earlier, multiple studies have reported AABW cooling in the North Atlantic in the twenty-first century[27,31,40] instead of warming. These conflicting reports result from relatively short time series and the inclusion of areas with substantial NADW content in their analyses, reflecting the NADW variability[10,27,41].

Abyssal ocean circulation in a warming planet

The consistently observed contraction of the AABW layer along the main Atlantic AABW pathway (that is, from the Weddell Sea through the Argentine, Brazil and western North Atlantic basins)[3,15,17,32,42], together with the confirmation of the weakening of the abyssal geostrophic flow (this study), strongly suggests that these are effects of reduction in the AABW production and export rates around and out of the Southern Ocean. This observational-only perspective of the phenomenon further corroborates the numerical results broadly explored in the past decades[18,20,25]. These numerical studies also showed that AABW anomalies are communicated northward on timescales shorter than abyssal advective timescales via wave propagation, suggesting the global abyssal circulation could rapidly adjust to a warmer planet in only a few decades.

Assuming the AABW spreading pathway between the Weddell Sea and 16° N between the Atlantic's western continental margins and western flank of MAR (≥13,000 km) and advective velocities between the maximum and average AABW flow speeds O (10^{-3}–10^{-2} m s^{-1}) (for example, Figs. 1c and 2a), we expect advective timescales varying between 40 and 400 years, implying that anomalies from the 1960s would only arrive in the North Atlantic subtropics in the early 2000s if advected at maximum AABW speeds. Although it is still unclear whether the production of AABW[25,42] in or processes decreasing the AABW export out of[43] the Weddell Sea is dominating the downstream abyssal AMOC weakening[23], the flow weakening happening since the 1980s[3,26] probably arrived in the North Atlantic Ocean through fast propagating topographic and planetary waves[20].

Notably, recent projections of the AABW flow reduction under the Intergovernmental Panel on Climate Change's high greenhouse gas emissions scenarios suggest it could increase the global abyssal heat content by 10 ZJ between 1990 and 2050[25]. Under the current warming rates, our results suggest around 10–15% of this excess heat could be in the abyssal western North Atlantic alone by 2050. Despite the relevance of the abyssal North Atlantic to the global heat budget, we report warming rates that are approximately half the trends observed below 4,500 m throughout the western South Atlantic and parts of the Southern Ocean[14,15,24,32,44]. This difference is probably due to the continuous vertical mixing between the AABW and NADW along their pathways, especially over the rough topography of the MAR's western flank where both vertical mixing[35,45,46] and AABW flow are stronger (Fig. 1c). Therefore, to accurately predict the AABW evolution and the abyssal ocean's contribution to Earth's heat and carbon budgets, climate models must accurately represent the abyssal water's subtle properties variations and account for the impact of small-scale motions on the large-scale flow.

Online content

Any methods, additional references, Nature Portfolio reporting summaries, source data, extended data, supplementary information, acknowledgements, peer review information; details of author contributions and competing interests; and statements of data and code availability are available at https://doi.org/10.1038/s41561-024-01422-4.

References

1. Orsi, A. H., Johnson, G. C. & Bullister, J. L. Circulation, mixing, and production of Antarctic Bottom Water. *Prog. Oceanogr.* **43**, 55–109 (1999).
2. Lumpkin, R. & Speer, K. Global ocean meridional overturning. *J. Phys. Oceanogr.* **37**, 2550–2562 (2007).
3. Johnson, G. C. Quantifying Antarctic Bottom Water and North Atlantic Deep Water volumes. *J. Geophys. Res.* **113**, C05027 (2008).
4. Johnson, G. C. et al. Global oceans: ocean heat content. *Bull. Am. Meteorol. Soc.* **99**, Si–S310 (2018).
5. Bagnell, A. & DeVries, T. 20th century cooling of the deep ocean contributed to delayed acceleration of Earth's energy imbalance. *Nat. Commun.* **12**, 4604 (2021).
6. Purkey, S. G. & Johnson, G. C. Warming of global abyssal and deep Southern Ocean waters between the 1990s and 2000s: contributions to global heat and sea level rise budgets. *J. Climate* **23**, 6336–6351 (2010).
7. Kouketsu, S. et al. Deep ocean heat content changes estimated from observation and reanalysis product and their influence on sea level change. *J. Geophys. Res.* **116**, C03012 (2011).
8. Zenk, W. & Morozov, E. Decadal warming of the coldest Antarctic Bottom Water flow through the Vema Channel. *Geophys. Res. Lett.* **34**, L14607 (2007).
9. Johnson, G. C., Purkey, S. G. & Toole, J. M. Reduced Antarctic meridional overturning circulation reaches the North Atlantic Ocean. *Geophys. Res. Lett.* **35**, L22601 (2008).
10. Desbruyères, D. G., Purkey, S. G., McDonagh, E. L., Johnson, G. C. & King, B. A. Deep and abyssal ocean warming from 35 years of repeat hydrography. *Geophys. Res. Lett.* **43**, 10,356–10,365 (2016).
11. Menezes, V. V., Macdonald, A. M. & Schatzman, C. Accelerated freshening of Antarctic Bottom Water over the last decade in the southern indian ocean. *Sci. Adv.* https://doi.org/10.1126/sciadv.1601426 (2017).
12. Purkey, S. G. et al. Unabated bottom water warming and freshening in the South Pacific ocean. *J. Geophys. Res.: Oceans* **124**, 1778–1794 (2019).
13. Johnson, G. C., Purkey, S. G., Zilberman, N. V. & Roemmich, D. Deep Argo quantifies bottom water warming rates in the southwest Pacific Basin. *Geophys. Res. Lett.* **46**, 2662–2669 (2019).
14. Strass, V. H., Rohardt, G., Kanzow, T., Hoppema, M. & Boebel, O. Multidecadal warming and density loss in the deep Weddell Sea, Antarctica. *J. Climate* **33**, 9863–9881 (2020).
15. Johnson, G. C. Antarctic Bottom Water warming and circulation slowdown in the Argentine Basin from analyses of deep Argo and historical shipboard temperature data. *Geophys. Res. Lett.* https://doi.org/10.1029/2022GL100526 (2022).
16. van Wijk, E. M. & Rintoul, S. R. Freshening drives contraction of Antarctic Bottom Water in the Australian Antarctic Basin. *Geophys. Res. Lett.* **41**, 1657–1664 (2014).
17. Purkey, S. G. & Johnson, G. C. Global contraction of Antarctic Bottom Water between the 1980s and 2000s. *J. Clim.* **25**, 5830–5844 (2012).
18. Masuda, S. et al. Simulated rapid warming of abyssal North Pacific waters. *Science* **329**, 319–322 (2010).
19. Nakano, H. & Suginohara, N. Importance of the eastern Indian Ocean for the abyssal Pacific. *J. Geophys. Res.: Oceans* **107**, 3219 (2002).
20. Patara, L. & Böning, C. W. Abyssal ocean warming around Antarctica strengthens the Atlantic overturning circulation. *Geophys. Res. Lett.* **41**, 3972–3978 (2014).
21. Khatiwala, S., Primeau, F. & Holzer, M. Ventilation of the deep ocean constrained with tracer observations and implications for radiocarbon estimates of ideal mean age. *Planet. Sci. Lett.* **325–326**, 116–125 (2012).
22. Solodoch, A. et al. How does Antarctic Bottom Water cross the Southern Ocean? *Geophys. Res. Lett.* https://doi.org/10.1029/2021GL097211 (2022).
23. Silvano, A. et al. Observing Antarctic Bottom Water in the Southern Ocean. *Front. Mar. Sci.* https://doi.org/10.3389/fmars.2023.1221701 (2023).

24. Campos, E. J. D. et al. Warming trend in Antarctic Bottom Water in the Vema Channel in the South Atlantic. *Geophys. Res. Lett.* https://doi.org/10.1029/2021GL094709 (2021).
25. Li, Q., England, M. H., Hogg, A. M., Rintoul, S. R. & Morrison, A. K. Abyssal ocean overturning slowdown and warming driven by Antarctic meltwater. *Nature* **615**, 841–847 (2023).
26. Frajka-Williams, E., Cunningham, S. A., Bryden, H. & King, B. A. Variability of Antarctic Bottom Water at 24.5° N in the Atlantic. *J. Geophys. Res.: Oceans* https://doi.org/10.1029/2011JC007168 (2011).
27. Desbruyères, D., McDonagh, E. L., King, B. A. & Thierry, V. Global and full-depth ocean temperature trends during the early twenty-first century from Argo and repeat hydrography. *J. Clim.* **30**, 1985–1997 (2017).
28. Schmitz, W. J. & McCartney, M. S. On the North Atlantic circulation. *Rev. Geophys.* **31**, 29–49 (1993).
29. Talley, L. D., Pickard, G. L., Emery, W. J. & Swift, J. H. *Descriptive Physical Oceanography: An Introduction* 6th edn (Academic Press, 2011).
30. Herrford, J., Brandt, P. & Zenk, W. Property changes of deep and bottom waters in the western tropical Atlantic. *Deep Sea Res. Part I* **124**, 103–125 (2017).
31. Cunningham, S. A. & Alderson, S. Transatlantic temperature and salinity changes at 24.5° N from 1957 to 2004. *Geophys. Res. Lett.* https://doi.org/10.1029/2007GL029821 (2007).
32. Johnson, G. C., Cadot, C., Lyman, J. M., McTaggart, K. E. & Steffen, E. L. Antarctic Bottom Water warming in the Brazil Basin: 1990s through 2020, from WOCE to Deep Argo. *Geophys. Res. Lett.* https://doi.org/10.1029/2020GL089191 (2020).
33. Johnson, G. C., Robbins, P. E. & Hufford, G. E. Systematic adjustments of hydrographic sections for internal consistency. *J. Atmos. Oceanic Technol.* **18**, 1234–1244 (2001).
34. Wright, W. R. Northward transport of Antarctic Bottom Water in the western Atlantic Ocean. *Deep Sea Res.* **17**, 367–371 (1970).
35. Mauritzen, C., Polzin, K. L., McCartney, M. S., Millard, R. C. & West-Mack, D. E. Evidence in hydrography and density fine structure for enhanced vertical mixing over the Mid-Atlantic Ridge in the western Atlantic. *J. Geophys. Res.* **107**, 3147 (2002).
36. Kanzow, T. *Monitoring the Integrated Deep Meridional Flow in the Tropical North Atlantic*. Ph.D. thesis, Christian-Albrechts Universität Kiel (2004).
37. Spall, M. A. Wave-induced abyssal recirculations. *J. Mar. Res.* **52**, 1051–1080 (1994).
38. Biló, T. C. & Johns, W. E. The Deep Western Boundary Current and adjacent interior circulation at 24°–30° N: mean structure and mesoscale variability. *J. Phys. Oceanogr.* **50**, 2735–2758 (2020).
39. Kanzow, T., Send, U., Zenk, W., Chave, A. D. & Rhein, M. Monitoring the integrated deep meridional flow in the tropical North Atlantic: long-term performance of a geostrophic array. *Deep Sea Res. Part I* **53**, 528–546 (2006).
40. Limeburner, R., Whitehead, J. A. & Cenedese, C. Variability of Antarctic Bottom Water flow into the North Atlantic. *Deep Sea Res. Part II* **52**, 495–512 (2005).
41. Desbruyères, D. G. et al. Warming-to-cooling reversal of overflow-derived water masses in the Irminger Sea during 2002–2021. *Geophys. Res. Lett.* **49**, 1–10 (2022).
42. Zhou, S. et al. Slowdown of Antarctic Bottom Water export driven by climatic wind and sea-ice changes. *Nat. Clim. Change* **13**, 701–709 (2023).
43. Meredith, M. P., Garabato, A. C. N., Gordon, A. L. & Johnson, G. C. Evolution of the deep and bottom waters of the Scotia Sea, Southern Ocean, during 1995–2005*. *J. Clim.* **21**, 3327–3343 (2008).
44. Meinen, C. S., Perez, R. C., Dong, S., Piola, A. R. & Campos, E. J. D. Observed ocean bottom temperature variability at four sites in the northwestern Argentine Basin: evidence of decadal deep/abyssal warming amidst hourly to interannual variability during 2009–2019. *Geophys. Res. Lett.* https://doi.org/10.1029/2020GL089093 (2020).
45. Polzin, K. L., Toole, J. M., Ledwell, J. R. & Schmitt, R. W. Spatial variability of turbulent mixing in the abyssal ocean. *Science* **276**, 93–96 (1997).
46. St Laurent, L. C. & Thurnherr, A. M. Intense mixing of lower thermocline water on the crest of the Mid-Atlantic Ridge. *Nature* **448**, 680–683 (2007).

Methods

Mooring records

To study the AABW inflow (that is, transport) to the subtropical North Atlantic, we analyzed data from two hydrographic moorings between February 2000 and December 2020 from the Meridional Overturning Variability Experiment (MOVE) at 16° N[47]. These moorings provide measurements down to 5000 m depth near the western boundary and the western flank of the MAR (Fig. 1, Supplemental Information Fig. S1, and Table S1). In addition, to aid in the interpretation of the results and the transport calculations across 16°N, we used nine Guyana Abyssal Gyre Experiment (GAGE) currentmeter moorings deployed between the MOVE moorings[39,48]. The GAGE observations are located between ~ 1600-5200 m of the water column and range from February 2000 to April 2002 (Fig. 1c, Supplemental Information Fig. S1, and Table S2).

Then, to interpret temperature variability in the North Atlantic subtropics, we analysed near-bottom (~5,000 m) temperature records at two additional locations farther north (24.5° N–26.5° N) at the MAR's western flank and near the western boundary (Figs. 1a, 4a and Supplementary Table 3). At MAR's western flank, we used temperature, conductivity and pressure records between April 2004 and August 2018 from a mooring from the Rapid Climate Change Meridional Overturning Circulation programme (RAPID)[49,50]. Near the western boundary, temperature records between September 2004 and March 2021 were from a Pressure Equipped Inverted Echo Sounder's (PIES) internal temperature sensor. The PIES' records were obtained from the Western Boundary Current Time Series (WBTS) programme[51]. Details about the datasets and data accuracy can be found in the Supplementary Information under 'Moored instrumentation'.

Cruise hydrographic data and auxiliary data products

We utilized quality-controlled hydrographic CTD, Deep Argo and climatological profiles from various sources to map the AABW layer and study the abyssal temperature variability. At 16° N, we relied on CTD profiles from two cruises initiated in February 2000 and 2002 servicing the MOVE and GAGE moorings[48] (Fig. 1b,c). Along 24.5° N–26.5° N latitudes, we analysed CTD profiles from six occupations of the transatlantic historical A05 line between 1998 and 2020 that started as part of the World Ocean Circulation Experiment (WOCE) and continued under the coordination of the International Global Ocean Ship-Based Hydrographic Investigations Program (GOSHIP). Additionally, we included 28 CTD transects repeated between 2000 and 2021, spanning 70° W–77° W along 26.5° N as part of the WBTS programme[51], and profiles from seven cruises servicing the RAPID mooring on the western flank of the MAR since 2004 (Fig. 1a shows the area covered by the observations). To strengthen our CTD data analysis, we also used a total of 36 Argo quality-controlled temperature and salinity profiles from deep Argo floats[52] obtained between March 2017 and May 2021 as additional abyssal potential temperature measurements (grey box in Fig. 1a for reference). These floats take measurements down to a depth of 6,000 m. Further details about these datasets and their respective accuracy can be found in the Supplementary Information under 'CTD measurements accuracy and Deep Argo data'.

Finally, we analysed the climatological temperature and salinity within the abyssal North Atlantic from the World Ocean Atlas (WOA) 2018 product[53,54]. This product has a horizontal resolution of 0.25° × 0.25°, global coverage, and 102 vertical levels ranging from 0 to 5,500 m depth. The topography data displayed and mentioned throughout this article is the General Bathymetric Chart of the Oceans (GEBCO) 30-arc second resolution gridded topographic product[55].

Geostrophic shear and AABW transports at 16° N

In the North Atlantic, the AABW is commonly defined as waters within the potential temperature layer colder than 1.8 °C (refs. 9,26,56). To assess the AABW flow variability, we estimated the geostrophic volume transport of waters within this cold layer at 16° N across the MOVE array (Fig. 1) between 2000 and 2020. We chose 16° N due to the high-temporal resolution of the MOVE array measurements (that is, 5–10 minutes) compared to other available datasets. This way, we avoid aliasing problems of transport variability analysis on subinertial timescales. It is worth mentioning that we do not attempt to estimate the AABW transports using the GAGE moorings because the array was not designed to resolve the lateral structure of the boundary currents at 16° N, compromising absolute transport estimates from directly observed velocities[36].

To do this, we first vertically interpolated the temperature and salinity measurements at each MOVE mooring location using the Piecewise Cubic Hermite Interpolating Polynomial[57] to a uniform 20-m grid. Throughout the consistent 13 MOVE deployments (Supplementary Table 1), this procedure allowed us to obtain temperature and salinity at the same depths in both locations between 2000 and 2020 and vertically interpolate over short data gaps generated by sporadic instrument failures. Then, we computed the dynamic height profiles at each mooring location, allowing us to use the Dynamic Method[29] to estimate the zonally averaged geostrophic velocity profile (that is, net geostrophic flow profile) relative to 4,500 m between the two moorings. The 4,500-m level represents the average depth of the approximate NADW–AABW interface at 16° N (that is, 1.8 °C isotherm). Finally, we performed a vertical extrapolation to obtain the flow below 5,000 m before integrating the velocity between the moorings and below 4,500 m ('The vertical extrapolation below 5,000 m' section provides details).

After obtaining a complete 4,500-m bottom zonally averaged geostrophic velocity profile at each time step, we computed the horizontally integrated transport by multiplying the velocity by the average distance between the MOVE moorings (that is, ~1,000 km). Then, we vertically integrated this transport below 4,500 m using a trapezoidal integration scheme to obtain the final AABW transports across 16° N in Sverdrups (that is, $1\ \mathrm{Sv} = 1 \times 10^6\ \mathrm{m^3\ s^{-1}}$).

The referencing at 4,500 m

The northward AABW flow opposes the southward NADW flow within lighter and warmer layers of the water column[29,56]. Therefore, we chose the commonly assumed NADW–AABW interface in the North Atlantic—that is, 1.8 °C isotherm mean depth of 4,500 m—as the reference level to obtain the closest geostrophic velocities to the ocean's absolute velocity as possible at 16° N. However, accurately estimating the mean 1.8 °C isotherm depth based solely on the mooring data was difficult due to the approximately 1,000 km distance between the moorings (Fig. 1b). To address this issue, we used high-resolution CTD transects obtained during 2000 and 2002 cruises servicing the MOVE and GAGE moorings. On the basis of these cruises, we found that the average depth of the 1.8 °C isotherm between the MOVE moorings is approximately 4,500 m (for example, Fig. 1b), which is also supported by the WOA18 climatology at 16° N.

The referencing procedure corresponds to the primary source of uncertainty in geostrophic estimates[58]. Therefore, it is imperative to examine the referencing limitations and uncertainties. Previous analysis of the first few years of MOVE hydrographic records and the MOVE–GAGE currentmeter measurements obtained between 2000 and 2002 indicated that an average level of no motion could exist around 4,300 m (refs. 36,48). Because 4,300 m is relatively close to 4,500 m compared with the thickness of the AABW layer (~4,500–6,000 m, Fig. 1b,c), the mean average AABW transport and AMOC weakening referenced at ~4,300 m agrees with our estimates within uncertainties. In addition, the 4,500 m corresponds to the average level of no motion from geostrophic estimates done within numerical simulations[59].

Although the AABW layer is mostly below 4,500 m, a constant level of no motion has never been found in the real ocean. For example, under the current abyssal warming scenario, where the AABW layer

is shrinking over the years[9], assuming a fixed level of no motion may not be appropriate because the depth of zero velocity may be deepening, resulting in a more substantial weakening of the transport. In the Supplementary Information ('Sensitivity test for the geostrophic referencing at the constant depth of 4,500 m at 16° N'), our simple variability analysis of the 1.8 °C isotherm depth shows that the relatively modest vertical motions of this interface (standard deviation of ~47 m and trend of ~1.4 m per year) do not impose substantial changes in the AABW transport trends or its variability on interannual timescales (Supplementary Fig. 2), highlighting the robustness of our results. In contrast, transport oscillations on shorter timescales are substantially impacted by the choice of a constant level of no motion, suggesting this method might not be suitable on daily to seasonal timescales. Finally, choosing a substantially deeper reference level can modify the transport variability characteristics in all timescales due to the proximity to the maximum AABW velocity (Supplementary Fig. 3). To conclude, for the purpose of this study, a constant 4,500 m is a reasonable reference choice, given the evidence from the previous studies, the documented AABW boundaries at 16° N and sensitivity analyses discussed in the Supplementary Information.

The vertical extrapolation below 5,000 m

The MOVE array moorings do not observe areas deeper than 5,000 m. According to the GEBCO topography and previously reported topographic data[39,48,59,60], the average water column depth across the MOVE array is approximately 5,400 m (Fig. 1a,b), with a valley reaching almost 6,000 m. Therefore, a substantial portion of the abyssal flow is not directly observed by the MOVE array. Not resolving the full abyssal ocean is common for most AMOC monitoring arrays.

Notably, velocity distributions (Figs. 1c and 2a), previous analysis of moored records at 16° N (refs. 36,48) and numerical estimates of the net flow across 16° N (ref. 59) suggest that the AABW maximum northward flow is located around 5,000–5,200 m. Therefore, because we observe the velocities near 5,000 m, it is possible to estimate the unresolved transport assuming a realistic velocity vertical shear below 5,000 m. To estimate the abyssal shear and the unresolved transport, we determined the depth range over which the AABW net flow decays to zero using the GAGE currentmeter moorings and high-resolution CTD records. Then, we vertically interpolated the geostrophic profiles between the deepest MOVE measurement and this near-bottom zero-velocity depth.

Like the MOVE moorings, the GAGE instruments do not cover the entire water column. However, because the GAGE observations largely overestimate the net AABW maximum velocities due to its well-known lateral resolution problem[36], we can extrapolate the currentmeter velocity profiles at each GAGE mooring location to obtain an overestimate of the net flow near the bottom and its vertical shear. We obtained an upper and lower limit for the shear below 5,200 m by applying a Dirichlet (that is, no-slip condition $v = 0$ m s^{-1} at the sea floor) and a Newman (that is, full-slip condition $\partial v/\partial z = 0$ s^{-1} at the sea floor) velocity boundary conditions at the bottom. Supplementary Fig. 4 shows the horizontally averaged GAGE velocity profiles. For both conditions, the velocity profile decays to values below 1×10^{-3} m s^{-1} at approximately 5,600 m and to virtually zero at 5,800 m. Additionally, the geostrophic velocity profiles referenced at 4,500 m from the high-resolution CTDs show similar velocity values at these depths with zero-velocity crossing depth at approximately 5,700 m (Fig. 2a).

To determine the AABW transports from the MOVE array, we assumed constant zero crossing velocities at approximately 5,700 m, with 100 m of uncertainty propagated across our transport calculations. We then used a shape-preserving spline scheme[61] to vertically interpolate the resulting geostrophic velocity profile for the final velocity integration. Note that our extrapolation scheme does not account for minor nuances in the geostrophic profiles below 5,000 m, such as velocity sign inversions (Fig. 2a). However, the AABW transports obtained from both the 2000 (2.96 Sv) and 2002 (2.45 Sv) CTD-based transports fall within the 95% confidence interval of the average transport from the MOVE moorings. When comparing the CTD transect transport in 2002 with the concurrent MOVE mooring-based transport, the values agree within the uncertainties. Unfortunately, the CTD transect in 2000 was obtained before the MOVE array became fully operational, preventing us from directly comparing the CTD-based with the mooring-based transports.

The geostrophic shear variability decomposition

To assess the contributions of the hydrographic properties variability to the long-term vertical geostrophic shear trend (Fig. 3c,d), we calculated the shear time series at each depth due to the density changes near the MAR (MAR), temperature changes near the MAR (MAR$_\theta$) and density changes within the DWBC domain (DWBC). To do so, we replaced the temperature and salinity time series with their respective constant 20-year-long time average as follows:

- MAR: constant density profile at the western boundary mooring site.
- MAR$_\theta$: constant density profile at the western boundary mooring and constant salinity at the MAR mooring.
- DWBC: constant density profile at the MAR mooring site.

Potential temperature trends decomposition, ocean heat content and thermal expansion of the seawater

To quantitatively attribute the portion of the potential temperature (θ) trends associated with the isopycnals vertical displacements at each depth, we decomposed θ temporal anomalies into heave (that is, θ anomalies at a fixed pressure due to isopycnal displacement) and spice (θ anomalies along density surfaces)[62]. Temperature profiles along the WOCE/GOSHIP A05 transect and from the MOVE mooring near the MAR were interpolated onto a 5×10^{-4} kg m^{-3} resolution neutral density (γ_n) vertical grid. Then we computed the heave and spice terms in density space following equation (1)[41,63].

$$\theta' = \theta'\Big|_{\gamma_n} + z' \times \frac{\partial \theta}{\partial z}\Big|_{\gamma_n}, \quad (1)$$

where the first and second terms of the right-hand side are the spice and heave θ components, respectively, and z is depth. The term $\frac{\partial \theta}{\partial z}$ is the background (that is, time averaged) thermal gradient. After we estimated the θ terms, we re-interpolated them to the original vertical depth coordinates such that temporal linear trends could be calculated.

To perform our rough estimates of the increase of the abyssal ocean heat content (ΔQ) and its contribution to sea-level rise (SLR) between 2000 and 2020, we solved the well-known and widely used equations (2) and (3)[6].

$$\Delta Q = \int_V \Delta\theta(z) \times \rho \times C_p dV, \quad (2)$$

where V is the AABW volume, ρ is the water density, C_p is the seawater's isobaric heat capacity and $\Delta\theta(z)$ is the potential temperature change profile over 20 years.

$$\mathrm{SLR} = \frac{\int_V \Delta\theta(z) \times \alpha dV}{A}, \quad (3)$$

where α is the thermal expansion of the seawater and A is the North Atlantic area covered by AABW. All parameters from equations (2) and (3) were calculated using the WOA18 climatology in the western North Atlantic, except the $\Delta\theta(z)$. We obtained AABW's area and volume based on the climatological distribution of the waters colder than 1.8 °C (that is, west of the MAR's crest). Whereas the area corresponds to the areal

extent of waters colder than 1.8 °C, the volume was calculated as the sum of the AABW volume in each WOA18's grid cell with 0.25° × 0.25° of area. At each grid cell, the AABW thickness was defined as the distance between the 1.8 °C isotherm and local bottom depth from GEBCO. Then we calculated the profile $\Delta\theta(z)$ by time integrating the CTD-based temperature trend profile at 24.5° N shown in Fig. 4b (green line) over 20 years. We obtained similar results by assuming an uniform average warming rate of ~1 m°C per year between 4,500-m bottom in the western North Atlantic south of 40° N (that is, northernmost AABW penetration in Fig. 1a).

Seawater properties and dynamic height

We estimated all seawater parameters and properties (that is, θ, ρ, C_p, α) and the dynamic height for the geostrophic estimates using the TEOS-10 Python Gibbs Seawater Oceanographic 3.4.2 software[64], except γ_n. Therefore, all properties and parameters were calculated as a function of conservative temperature and absolute salinity required by the TEOS-10 subroutines. We chose to show our results in terms of θ and practical salinity for a convenient comparison with previous studies and discussion of the results. Additionally, results from equations (2) and (3) do not depend on the temperature scale in the abyssal ocean, being the ΔQ and SLR values several orders of magnitude larger than the difference between the results using the different temperature scales. Although the γ_n capabilities were discontinued from this particular Python package, the previous versions still have the γ_n calculation routines following the methodology of ref. 65.

Unfortunately, PIES and 18 of the Deep Argo profiles did not provide salinity records, so we cannot readily use the available software and data to estimate θ from these records. The former does not have a conductivity sensor for salinity calculations, and the latter presents conductivity measurements below 4,500 m flagged as bad or missing data by the quality control procedure[52]. Because the range of salinity values below 3,000 m is small (34.84–34.89), assuming a constant salinity value to convert in situ temperature records to θ results in errors smaller than 4×10^{-3} m°C below 4,500 m, which is orders of magnitude smaller than the observed temperature variability. Therefore, to convert the PIES and Deep Argo in situ temperature profiles in θ, we used the 3,000–6,000 m average salinity from the CTDs along A05 (Supplementary Information under 'Estimating potential temperature').

Filtering procedure, computation of trends and trends uncertainties

We isolated the interannual and longer timescales in our time series by low pass filtering them. Our filtering procedure consists of a fourth-order Butterworth filter[66] with a cut-off period of 18 months[67]. In addition, we fitted linear models to our time series using standard unweighted least squares regressions[66] to estimate the AABW transport, velocity shear and temperature trends.

Uncertainties and their respective confidence intervals discussed throughout this study represent the standard errors of each statistical parameter unless explicitly stated otherwise. For trends and low pass filtering procedures, we calculated the standard errors using the distribution of the residuals between the original time series and the linear model or filtered series[13,41]. Finally, due to the vigorous interannual variability of the AABW geostrophic transport (Fig. 2b), its non-normal distribution (Supplementary Fig. 5a and Supplementary Table 4) and the presence of serial correlations in the series (Supplementary Fig. 5b), additional trend estimate methods and significance tests are required to assess the robustness of our calculations further. Therefore we used the pyMannKendall software[68] to apply different versions of the non-parametric Mann Kendall (MK) trends statistical tests[69–71] to quantify the robustness of our calculations. All tests suggested AABW transport trends are significant at the 95% confidence level with p values smaller than 0.01 (Supplementary Table 5). Details about our error analyses and statistical tests can be found in the Supplementary Information under 'Uncertainties'.

Data availability

All data used in this study are freely available and can be accessed as follows: MOVE (link for the OceanSITES Global Data Assembly Center Public FTP Server can be found at https://mooring.ucsd.edu/move/ (ref. 72)); GAGE (https://doi.org/10.17604/5jd9-7f77 (ref. 73)); WOCE and GOSHIP A05 line (https://cchdo.ucsd.edu/ (ref. 74)); RAPID (https://www.bodc.ac.uk/data/bodc_database/nodb/ (ref. 75)); Deep Argo (https://doi.org/10.17882/42182 (ref. 76)); WBTS (link for the AOML-NOAA's public FTP server can be found at https://www.aoml.noaa.gov/phod/wbts/data.php (ref. 77)); WOA18 (https://www.ncei.noaa.gov/data/oceans/woa/WOA18/DATA/ (ref. 78)); GEBCO (https://www.gebco.net/data_and_products/gridded_bathymetry_data/ (ref. 55).

Code availability

All the codes used in this study are freely available in public repositories. As mentioned in Methods, all relevant seawater parameters, properties and dynamic height were computed using the Python Gibbs Seawater Oceanographic 3.4.2 software available at https://www.teos-10.org/software.htm#1. The γ_n routine can be found at http://www.teos-10.org/preteos10_software/gamma_GP.html. The Python pyMannKendall software for the MK trends statistical tests is available at https://github.com/mmhs013/pyMannKendall/tree/v1.1. Finally, all data handling, mathematical operations, data interpolation and data filtering procedures were performed using standard functions found in the Xarray 0.20.1 (https://docs.xarray.dev/en/stable/), Numpy 1.21.5 (https://numpy.org/) and Scipy 1.7.3 (https://scipy.org/) Python 3 packages.

References

47. Send, U., Kanzow, T., Zenk, W. & Rhein, M. Monitoring the Atlantic Meridional Overturning Circulation at 16° N. *CLIVAR Exch.* **7**, 31–33 (2002).
48. Kanzow, T., Send, U. & McCartney, M. On the variability of the deep meridional transports in the tropical North Atlantic. *Deep Sea Res. Part I* **55**, 1601–1623 (2008).
49. Johns, W. E. et al. Variability of shallow and deep western boundary currents off the Bahamas during 2004–05: results from the 26° N RAPID–MOC array. *J. Phys. Oceanogr.* **38**, 605–623 (2008).
50. McCarthy, G. D. et al. Measuring the Atlantic Meridional Overturning Circulation at 26° N. *Prog. Oceanogr.* **130**, 91–111 (2015).
51. Meinen, C. S. et al. Variability of the Deep Western Boundary Current at 26.5° N during 2004–2009. *Deep Sea Res. Part II* **85**, 154–168 (2013).
52. Wong, A., Keeley, R., Carval, T. & the Argo Data Management Team *Argo Quality Control Manual for CTD and Trajectory Data* (Ifremer, 2023).
53. Locarnini, R. A. et al. *World Ocean Atlas 2018, Vol. 1: Temperature* NOAA Atlas NESDIS 81 (NOAA, 2018).
54. Zweng, M. M. et al. *World Ocean Atlas 2018, Vol. 2: Salinity* NOAA Atlas NESDIS 82 (NOAA, 2018).
55. GEBCO Compilation Group *GBCO 2020 Grid* (GEBCO, 2020).
56. McCartney, M. S., Bennett, S. L. & Woodgate-Jones, M. E. Eastward flow through the Mid-Atlantic Ridge at 11° N and its influence on the abyss of the eastern basin. *J. Phys. Oceanogr.* **21**, 1089–1121 (1991).
57. Gupta, M. M. Numerical methods and software (David Kahaner, Cleve Moler, and Stephen Nash). *SIAM Rev.* **33**, 144–147 (1991).
58. Johns, E., Watts, R. D. & Rossby, T. H. A test of geostrophy in the Gulf Stream. *J. Geophys. Res.* **94**, 3211–3222 (1989).

59. Danabasoglu, G. et al. Revisiting AMOC transport estimates from observations and models. *Geophys. Res. Lett*. https://doi.org/10.1029/2021GL093045 (2021).
60. Send, U., Lankhorst, M. & Kanzow, T. Observation of decadal change in the Atlantic meridional overturning circulation using 10 years of continuous transport data. *Geophys. Res. Lett*. https://doi.org/10.1029/2011GL049801 (2011).
61. Akima, H. A new method of interpolation and smooth curve fitting based on local procedures. *J. ACM* **17**, 589–602 (1970).
62. Bindoff, N. L. & Mcdougall, T. J. Diagnosing climate change and ocean ventilation using hydrographic data. *J. Phys. Oceanogr.* **24**, 1137–1152 (1994).
63. Häkkinen, S., Rhines, P. B. & Worthen, D. L. Heat content variability in the North Atlantic Ocean in ocean reanalyses. *Geophys. Res. Lett.* **42**, 2901–2909 (2015).
64. McDougall, T. J. & Barker, P. M. *Getting Started with TEOS-10 and the Gibbs Seawater (GSW) Oceanographic Toolbox* SCOR/IAPSO WG127 (Teos, 2011); http://www.teos-10.org/software.htm
65. Jackett, D. R. & McDougall, T. J. A neutral density variable for the world's oceans. *J. Phys. Oceanogr.* **27**, 237–263 (1997).
66. Emery, W. J. & Thomson, R. E. *Data Analysis Methods in Physical Oceanography* 3rd edn (Elsevier, 2001).
67. Biló, T. C., Straneo, F., Holte, J. & Le Bras, I. A. A. Arrival of new great salinity anomaly weakens convection in the Irminger Sea. *Geophys. Res. Lett.* **49**, e2022GL098857 (2022).
68. Hussain, M. & Mahmud, I. pymannkendall: a Python package for non parametric Mann Kendall family of trend tests. *J. Open Source Softw*. https://doi.org/10.5281/zenodo.3347253 (2019).
69. Mann, H. Nonparametric tests against trend. *Econometrica* https://doi.org/10.2307/1907187 (1945).
70. Kendall, M. *Rank Correlation Methods* 4th edn (Charles Griffin, 1975).
71. Yue, S. & Wang, C. The Mann–Kendall test modified by effective sample size to detect trend in serially correlated hydrological series. *Water Resour. Manage.* **18**, 201–218 (2004).
72. Send, U. & Lankhorst, M. Meridional overturning variability experiment. *Univ. California San Diego* https://mooring.ucsd.edu/move/ (2024).
73. Kanzow, T., Carrilho Bilo, T., Lankhorst, M. & Mauritzen, C. Guyana Abyssal Gyre Experiment (GAGE) current meter mooring ocean velocity records obtained between February 2000 and April 2002 at 16° N. *Univ. of Miami Libraries* https://doi.org/10.17604/5jd9-7f77 (2023).
74. WOCE and GOSHIP. CLIVAR and Carbon Hydrographic Data Office https://cchdo.ucsd.edu/ (2023).
75. RAPID. *National Oceanography Centre* https://www.bodc.ac.uk/data/bodc_database/nodb/ (2024).
76. Fumihiko, A. et al. Argo float data and metadata from Global Data Assembly Centre (Argo GDAC). *SEANOE* https://doi.org/10.17882/42182 (2024).
77. WBTS. *NOAA/OAR AOML* https://www.aoml.noaa.gov/phod/wbts/data.php (2024).
78. WOA18. *NCEI* https://www.ncei.noaa.gov/data/oceans/woa/WOA18/DATA/ (2019).

Acknowledgements

We thank the many scientists, engineers and mariners from many institutions worldwide who supported several projects that developed instruments and collected, processed and published the data we used in this work. That includes all CTD, Deep Argo and moored profiles. Without their collaboration and hard work, studies like this would not happen. We offer special thanks to M. Lankhorst and the MOVE team for providing the MOVE dataset, to the WBTS team (R. Smith, D. Volkov, R. Garcia, J. Hooper) for providing the WBTS mooring and CTD dataset, to C. Meinen, M. Harrison, D. Volkov, M. Le Henaff and L. Chomiak for the useful discussions. We also thank S.-K. Lee for reading the manuscript and providing useful comments. T.C.B., R.C.P. and S.D. gratefully acknowledge the funding from the National Oceanic and Atmospheric Administration (NOAA)'s Global Ocean Monitoring and Observing programme (FundRef number 100007298); NOAA's Climate Program Office, Climate Observations and Monitoring and Climate Variability and Predictability programmes under NOFO NOAA-OAR-CPO-2021-2006389 with additional NOAA Atlantic Oceanographic and Meteorological Laboratory support. Support for W.J.'s participation in the research was provided by the US National Science Foundation under grants OCE-1332978 and OCE-1926008. T.K. is funded by the EU's Horizon 2020 Research and Innovation Program under the grant agreement number 821001 (SO-CHIC) and therein is a contribution to its Work Packages 3 and 6. This study is further a contribution to the project T3 of the Collaborative Research Centre TRR 181 'Energy Transfers in Atmosphere and Ocean' funded by the Deutsche Forschungsgemeinschaft (DFG, German Research Foundation; project number 274762653). This research was carried out in part under the auspices of the Cooperative Institute for Marine and Atmospheric Studies, a cooperative institute of the University of Miami and the National Oceanic and Atmospheric Administration (NOAA), cooperative agreement NA 20OAR4320472.

Author contributions

T.C.B. led this study from the idea conception to the data analysis, results interpretation and paper writing. R.C.P. and S.D. contributed to the idea conception, results interpretation, discussion and paper preparation. W.J. and T.K. contributed to the data analysis, results interpretation and discussion and paper preparation.

Competing interests

The authors declare no competing interests.

Additional information

Extended data is available for this paper at https://doi.org/10.1038/s41561-024-01422-4.

Supplementary information The online version contains supplementary material available at https://doi.org/10.1038/s41561-024-01422-4.

Correspondence and requests for materials should be addressed to Tiago Carrilho Biló.

Peer review information *Nature Geoscience* thanks the anonymous reviewers for their contribution to the peer review of this work. Primary Handling Editor: Tom Richardson, in collaboration with the *Nature Geoscience* team.

https://doi.org/10.1038/s41561-024-01422-4

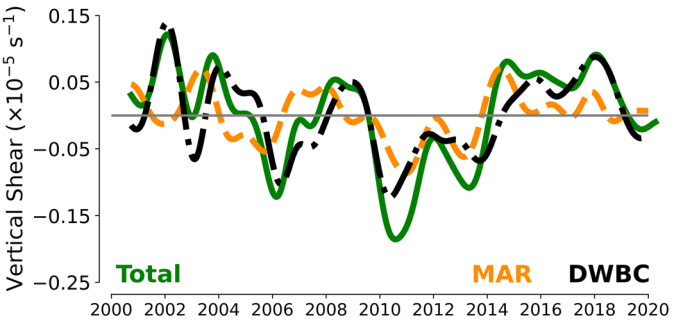

Extended Data Fig. 1 | MOVE data analysis showing that most of the vertical geostrophic shear variability below 4500 m at 16° N, ranging from interannual to decadal time scales, is driven primarily by density changes within the DWBC domain. Curves represent the detrended eighteen-month low-passed filtered abyssal geostrophic shear time anomalies series averaged between 4500-5000 m discussed in Fig. 3.

https://doi.org/10.1038/s41561-024-01422-4

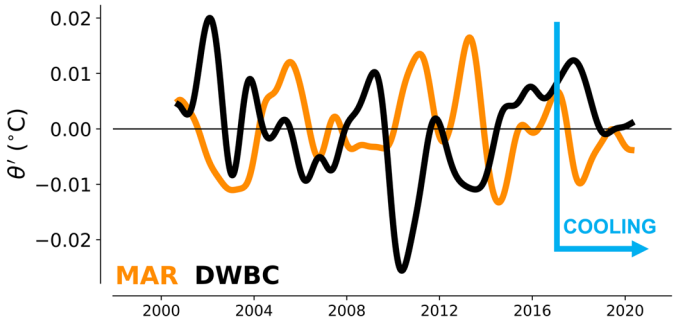

Extended Data Fig. 2 | MOVE potential temperature analysis showing the period after 2017 is characterized by colder temperatures than the previous years at 16° N (see blue arrows). Curves represent the detrended eighteen-month low-passed filtered potential temperature time anomalies series averaged between 4500-5000 m.